International Journal of Thermophysics, Vol. 26, No. 3, May 2005 (© 2005)
DOI: 10.1007/s10765-005-5583-5

A Molecular Dynamics Study for the Thermophysical Properties of Liquid Ti–Al Alloys

X. J. Han,[1] M. Chen,[1,2] and Z. Y. Guo[1]

Received July 18, 2004

Molecular dynamics simulations (MDS) employing an embedded-atom-method (EAM) are applied to calculate the density and specific heat of liquid Ti–Al alloys at temperatures above and below the melting temperature in a wide composition range. Both the temperature and composition dependences of these two properties are investigated. The excess volume of Ti–Al alloys is calculated from the predicted density, and shows a negative value. The specific heat of liquid Ti–Al alloys increases linearly with a decrease of temperature. Unlike the monotonic change of density with the addition of aluminum, the specific heat reaches its maximum value at the composition of Ti–50at%Al alloy. Thus, both the density and specific heat show highly non-ideal behaviors, indicating that Neumann–Kopp's rule does not apply.

KEY WORDS: density; EAM; molecular dynamics simulation; specific heat; Ti–Al alloy; undercooled liquid.

1. INTRODUCTION

Thermophysical properties, such as the specific heat and density of liquid alloys, especially in the undercooled regime, are of particular interest as they play important roles in understanding and defining the thermodynamic state of the system. Moreover, a detailed knowledge of these properties is indispensable to the improvement of casting techniques and computer modeling of the potential production routes [1]. This is of great significance for materials with high melting temperatures, such as for Ti aluminides.

Ti–Al alloys are attractive for a broad range of applications to aerospace and automobile engines due to their high strength, high melting

[1] Department of Engineering Mechanics, Tsinghua University, Beijing 100084, China.
[2] To whom correspondence should be addressed. E-mail: mchen@tsinghua.edu.cn

temperature, desirable oxidation and creep resistances, combined with low density [2–4]. Investigations on the thermophysical properties of such an alloy system in the liquid state are necessary for their future development. However, very limited experimental work has been done on this system due to the high melting temperature. For example, the melting temperature of Ti_3Al alloy is up to 1923 K. The experimental determination of the density and the specific heat at such a high temperature is quite challenging even for the electromagnetic levitation method, which has been widely used to measure these two parameters of liquid metals in recent years.

Molecular dynamics simulation (MDS) allows one to calculate properties that are difficult of access in experiments or hard to be measured with reasonable precision. Under extreme conditions, such as high temperature, high pressure, and high supercooling, MDS is especially suitable for predicting these quantities. MDS, as well as a potential model based on the embedded-atom-method (EAM), have been proved to be promising approaches to the simulation of metals; the latter was developed two decades ago and has been successfully applied to simulate the structure, surface, thermodynamic properties, and phase transformation of solid or liquid metals [5, 6].

Over the past decades, many simulation studies have been done on liquid Ti–Al alloys [7–9]. However, there is a lack of systematic investigations of the density and the specific heat of liquid Ti–Al alloys, especially in the undercooled regime. The objective of the present paper is to study the specific heat and density of this binary alloy system systematically with MDS. Ti, Ti–10at%Al, Ti_3Al, Ti–30at%Al, TiAl, Ti–70at%Al, $TiAl_3$ and Ti-90at%Al are selected as the compounds of interest.

2. EMBEDDED-ATOM-METHOD

The EAM is a procedure for designing a mathematical model of a metal, which was originally developed by researchers at Sandia National Laboratory [10, 11]. The basic equations of the EAM are

$$E_{\text{tot}} = \sum_i F_i(\rho_i) + \frac{1}{2} \sum_{i,j(i \neq j)} \phi_{i,j}\left(R_{i,j}\right) \tag{1}$$

$$\rho_i = \sum_{i \neq j} f_j\left(R_{i,j}\right) \tag{2}$$

where E_{tot} is the total internal energy, ρ_i is the electron density at atom i due to all other atoms, f_j is the electron density of atom j as a function of distance from its center, $R_{i,j}$ is the separation between atoms i and j,

$F_i(\rho_i)$ is the energy to embed atom i in an electron density ρ_{i} , and $\phi_{i,j}$ is a two-body central potential between atoms i and j.

The EAM model of Ti–Al binary alloy system was recently developed by Zope and Mishin [12]. According to this model, the electron density function, $f(r)$, and the pair interaction, $\phi(r)$, of aluminum are given in the forms,

$$f(r)=\varphi\left(\frac{r-r_c}{h}\right)\left\{A_0(r-r_0)^y e^{-\gamma(r-r_0)}\left[1+B_0 e^{-\gamma(r-r_0)}\right]+C_0\right\} \tag{3}$$

$$\phi(r)=\left[\frac{V_0}{(b_2-b_1)}\left(\frac{b_2}{z^{b_1}}-\frac{b_1}{z^{b_2}}\right)+\delta\right]\varphi\left(\frac{r-r_c}{h}\right) \tag{4}$$

where $z=r/r'$, A_0, B_0, C_0, r_0, r_c, h, y, γ, b_1, b_2, δ, V_0, and r' are fitting parameters, and $\varphi(x)$ is given by $\frac{x^4}{(1+x^4)}$ if x is less than zero; otherwise, $\varphi(x)=0$.

The embedding energy is obtained by equating the energy of aluminum to a modified version by the universal equation of state of Rose *et al.* [13]

$$E(r)=-E_0\left[1+\alpha x+\beta\alpha^3 x^3\frac{2x+3}{(x+1)^2}\right]e^{-\alpha x} \tag{5}$$

where $\alpha=\sqrt{9\Omega_0 B/E_0}$, $x=r/r_e-1$, and r, E_0, Ω_0, B, and r_e are the nearest-neighbor distance, cohesive energy, equilibrium atomic volume, bulk modulus, and equilibrium-nearest-neighbor distance, respectively.

$f(r)$ and $\phi(r)$ of Ti are described by

$$f(r)=\left[Ae^{-\alpha_1(r-r_0)^2}+e^{-\alpha_2(r-r_0')}\right]\varphi\left(\frac{r-r_c}{h}\right) \tag{6}$$

$$\phi(r)=\varphi\left(\frac{r-r_c}{h}\right)\left\{V_0 e^{-\beta_1 r_1}+V_0'\left[e^{-2\beta_2(r-r_1')}-2e^{\beta_2(r-r_1')}\right]+\delta\right\} \tag{7}$$

The embedding energy function of Ti is expressed as a polynomial

$$F(\rho)=F_0+\frac{1}{2}F_2(\rho-1)^2+q_0(\rho-1)^3+\sum_{i=1}^{3}B_i(\rho-1)^{i+3} \tag{8}$$

Here ρ is the electron density, and F_0 and F_2 are the embedding energy and its second derivative at equilibrium, respectively. F_0 and F_2 can be expressed in terms of the experimental values of E_0, Ω_0, and B;

$$F_0 = E_0 - \frac{1}{2}\sum_j N_j \varphi_j \tag{9}$$

and

$$\frac{1}{2}\sum_j N_j \varphi_j'' R_j^2 + F_2 \left(\sum_j N_j \rho_j R_j\right)^2 = 9B\Omega_0 \tag{10}$$

where j runs over coordination shells, N_j is the number of atoms on the jth coordination shell of radius R_j, while φ_j and φ_j'' are the pair-interaction energy and its second derivative evaluated at R_j.

The cross potential representing the interactions between Ti and Al atoms can also be represented in the form of Eq. (4). All the model parameters are listed in Table I.

Table I. Model Parameters of the Ti–Al System

Al		Ti		TiAl	
Parameter	Optimal value	Parameter	Optimal value	Parameter	Optimal value
r_c (Å)	6.724884	r_c (Å)	5.193995	r_c (Å)	5.7684889
h(Å)	3.293585	h (Å)	0.675729	h (Å)	0.619769
V_0 (eV)	-3.503182×10^3	V_0 (eV)	-3.401822×10^6	V_0 (eV)	−0.737065
r' (Å)	2.857784	r_1 (Å)	−8.825787	r_0 (Å)	2.845970
b_1	8.595076×10^{-2}	β_1 (Å^{-1})	5.933482	b_1	5.980610
b_2	5.012407×10^{-2}	V_0' (eV)	0.161862	b_2	5.902127
δ (eV)	3.750298×10^3	r_1' (Å)	3.142920	δ (eV)	0.078646
y	2.008047×10^1	β_2(Å^{-1})	2.183169		
γ (Å^{-1})	4.279852	δ	-0.601156×10^{-1}		
B_0(Å)	1.192727×10^5	A	3.656883×10^2		
C_0 (Å^{-3})	8.60297×10^{-2}	r_0 (Å)	-1.169053×10^1		
r_0 (Å)	0.5275494	r_0' (Å)	-2.596543×10^2		
β	0.00489	α_1(Å^{-1})	0.3969775×10^{-1}		
		α_2(Å^{-1})	5.344506×10^2		
		B_1	1.549707		
		B_2	−0.4471131		
		B_3	0.8594003×10^{-1}		

3. SIMULATION DETAILS

The density and specific heat are simulated by applying the MDS method under constant pressure and constant temperature (*NPT* ensemble). At the beginning of the simulation, 4000 atoms were arranged in a face-centered cubic box subject to periodic boundary conditions in three directions. The number of atoms of each type was assigned according to the atomic composition of Ti–Al alloys. During simulation, the pressure was set to zero, and the time step was set as 4.0×10^{-15} s. In order to get an equilibrium liquid state in the simulation, the system started at 2100 K, which is above the melting point. This temperature was kept constant for 50,000 steps. Then the quenching process with a cooling rate of $5 \times 10^{11}\,\mathrm{K \cdot s^{-1}}$ was carried out to calculate the enthalpy H and density ρ at 100 K intervals of temperature. At each temperature, 30,000 steps were carried out for equilibrium. Then 20,000 additional steps were taken to calculate the enthalpy and density. The simulation was stopped at 1300 K, which is 693, 463, 313, and 623 K lower than the melting temperature of Ti, TiAl, $TiAl_3$, and Ti_3Al, respectively. For pure Al, the stopping temperature corresponds to a superheat of 367 K.

According to Andersen's *NPT* algorithm, the length of the simulated cell is obtained. Thus, the density can be derived from its definition. The specific heat is determined from the differential of the enthalpy;

$$C_p = \frac{dH(T)}{dT} = \frac{d(E + PV)}{dT} \tag{11}$$

where E is the internal energy, i.e., the sum of the kinetic energy and potential energy, P is the pressure, and V is the volume of the simulated system.

4. RESULTS AND DISCUSSIONS

Figure 1 presents the predicted density of Ti–Al alloys vs. temperature. Data analysis shows that the density of pure liquid aluminum is represented by a second-order polynomial function of temperature T,

$$\rho = A + B_1 T + B_2 T^2\,\mathrm{g \cdot cm^{-3}} \tag{12}$$

whereas the density of other Ti–Al alloys can be well described by a linear function of temperature. The fitting parameters A, B_1, and B_2 are listed in Table II. Such a temperature dependence of pure liquid aluminum is not surprising. As Iida and Guthrie [14] pointed out, the experimentally

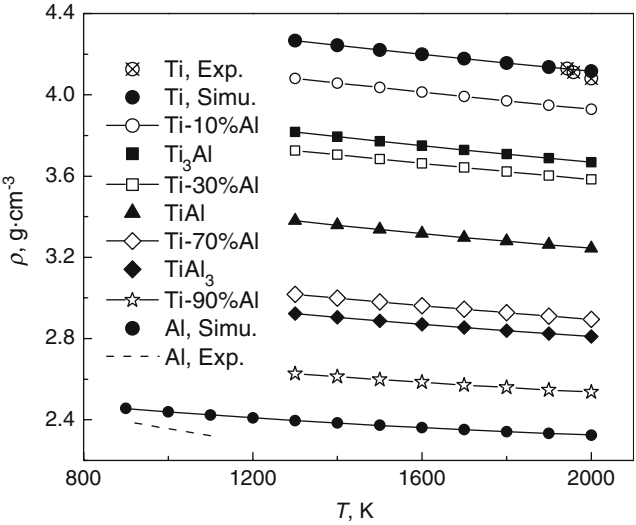

Fig. 1. Density of Ti–Al alloys at different temperatures.

Table II. Fitting Parameters for the Density of Ti–Al Alloys

Alloy	A $(g \cdot cm^{-3})$	B_1 $(g \cdot cm^{-3} \cdot K^{-1})$	B_2 $(g \cdot cm^{-3} \cdot K^{-2})$
Ti	4.5454	-2.1555×10^{-4}	0.0000
Ti–10at%Al	4.3636	-2.1819×10^{-4}	0.0000
Ti_3Al	4.0902	-2.1203×10^{-4}	0.0000
Ti–30at%Al	3.9886	-2.0324×10^{-4}	0.0000
TiAl	3.6264	-1.9206×10^{-4}	0.0000
Ti–70at%Al	3.2459	-1.7640×10^{-4}	0.0000
$TiAl_3$	3.1304	-1.6128×10^{-4}	0.0000
Ti–90at%Al	2.7932	-1.2958×10^{-4}	0.0000
Al	2.6350	-2.3635×10^{-4}	4.0819×10^{-8}

observed linear temperature variation of pure liquid metal may not be precisely true, and if the measurement had been made over a wider temperature range, some curvatures would have been probable.

In order to evaluate deviations between the predictions and experimental data, the density of pure liquid titanium and aluminum near their melting points are also superimposed upon Fig. 1. Near the melting point, the predicted density of titanium is in excellent agreement with

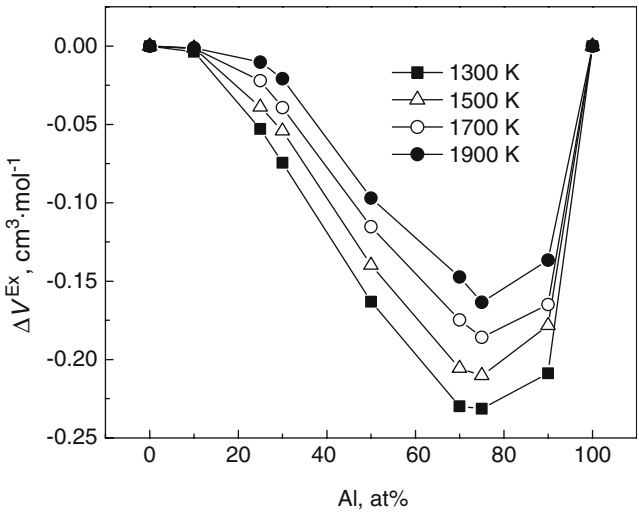

Fig. 2. Excess volme ΔV^{Ex} of Ti–Al.

experimental data [14], the difference being less than 0.3%. For aluminum, the deviation is about 3%. The deviations of the calculated densities of other Ti–Al alloys are not evaluated due to the lack of experimental data of the liquid state.

The excess volume can be calculated from the predicted density data of Ti–Al alloys according to the following expression [14],

$$\Delta V^{Ex} = [x_1 M_1 + x_2 M_2]/\rho_A - [x_1 M_1/\rho_1 + x_2 M_2/\rho_2] \tag{13}$$

where subscript 1 refers to Ti and 2 to Al, ρ_A is the alloy density, and x_i, M_i, and ρ_i are the atomic fraction, atomic weight, and density of components 1 and 2, respectively. The calculated ΔV^{Ex} of Ti–Al alloys are depicted in Fig. 2. For clarity, only ΔV^{Ex} at 1300, 1500, 1700, and 1900 K are illustrated. Obviously, Ti–Al alloys exhibit a negative excess volume and the lower the temperature, the smaller the excess volume. This means that liquid Ti–Al alloys deviate from the ideal solution. Moreover, a decrease of temperature strengthens the degree of this deviation.

Figure 3 illustrates the enthalpy of the Ti–Al alloys at the simulated temperatures. For clarity, only the enthalpy of Ti, Ti_3Al, TiAl, $TiAl_3$ and Al is presented. The enthalpy of Ti–Al alloys can be represented by a second-order polynomial function of the temperature,

$$H = H_0 + H_1 T + H_2 T^2 \ \mathrm{J \cdot mol^{-1}} \tag{14}$$

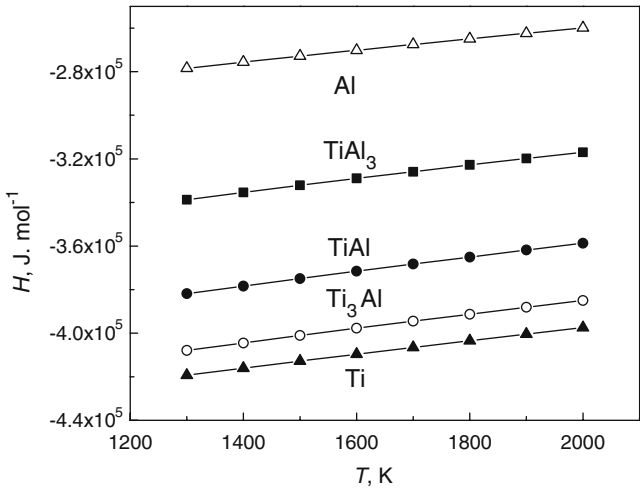

Fig. 3. Calculated enthalpy of Ti–Al alloys.

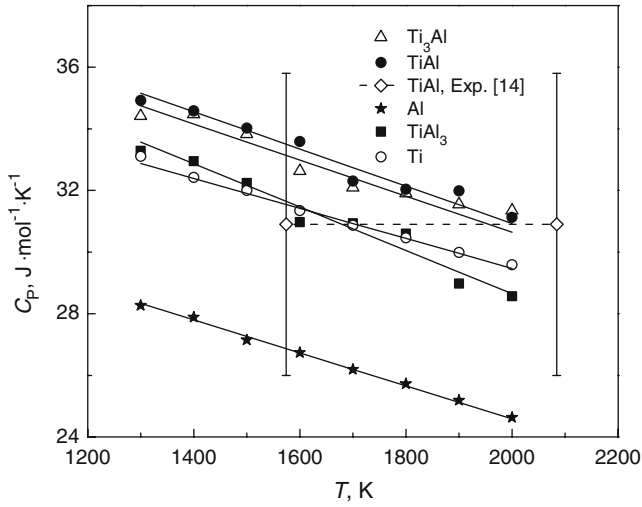

Fig. 4. Specific heat of Ti–Al alloys at different temperatures.

The fitting parameters are listed in Table III. From the first derivative of the enthalpy, the specific heat of Ti–Al alloys can be obtained and is illustrated in Fig. 4. Similar to the case of the enthalpy, the specific heats of Ti–10%Al, Ti–30%Al, Ti–70%Al and Ti–90%Al, are not superimposed on the figure. The specific heat is linearly related to the temperature:

Table III. Fitting Parameters for the Enthalpy of Ti–Al Alloys

Alloy	H_0(J·mol^{-1})	H_1(J·mol^{-1}·K^{-1})	H_2(J·mol^{-1}·K^{-2})
Ti	-4.661×10^5	39.193	-2.430×10^{-3}
Ti–10%Al	-4.649×10^5	40.681	-2.630×10^{-3}
Ti_3Al	-4.580×10^5	42.362	-2.930×10^{-3}
Ti–30%Al	-4.530×10^5	41.063	-2.540×10^{-3}
TiAl	-4.327×10^5	43.011	-3.020×10^{-3}
Ti–70%Al	-3.996×10^5	44.104	-3.760×10^{-3}
$TiAl_3$	-3.883×10^5	42.725	-3.520×10^{-3}
Ti–90%Al	-3.491×10^5	38.756	-3.110×10^{-3}
Al	-3.197×10^5	35.303	-2.680×10^{-3}

$$C_{P,\mathrm{Ti}} = 39.193 - 4.860 \times 10^{-3} T \ \ \mathrm{J \cdot mol^{-1} \cdot K^{-1}} \tag{15}$$

$$C_{P,\mathrm{Ti-10\%Al}} = 40.681 - 5.260 \times 10^{-3} T \ \ \mathrm{J \cdot mol^{-1} \cdot K^{-1}} \tag{16}$$

$$C_{P,\mathrm{Ti_3Al}} = 42.362 - 5.860 \times 10^{-3} T \ \ \mathrm{J \cdot mol^{-1} \cdot K^{-1}} \tag{17}$$

$$C_{P,\mathrm{Ti-30\%Al}} = 41.063 - 5.080 \times 10^{-3} T \ \ \mathrm{J \cdot mol^{-1} \cdot K^{-1}} \tag{18}$$

$$C_{P,\mathrm{TiAl}} = 43.011 - 6.040 \times 10^{-3} T \ \ \mathrm{J \cdot mol^{-1} \cdot K^{-1}} \tag{19}$$

$$C_{P,\mathrm{Ti-70\%Al}} = 44.104 - 7.520 \times 10^{-3} T \ \ \mathrm{J \cdot mol^{-1} \cdot K^{-1}} \tag{20}$$

$$C_{P,\mathrm{TiAl_3}} = 42.725 - 7.040 \times 10^{-3} T \ \ \mathrm{J \cdot mol^{-1} \cdot K^{-1}} \tag{21}$$

$$C_{P,\mathrm{Ti-90\%Al}} = 38.756 - 6.220 \times 10^{-3} T \ \ \mathrm{J \cdot mol^{-1} \cdot K^{-1}} \tag{22}$$

$$C_{P,\mathrm{Al}} = 35.303 - 5.360 \times 10^{-3} T \ \ \mathrm{J \cdot mol^{-1} \cdot K^{-1}} \tag{23}$$

In order to estimate how reasonable the predicted specific heats of Ti–Al alloys are, the experimentally determined C_P of Ti–50at% Al alloy

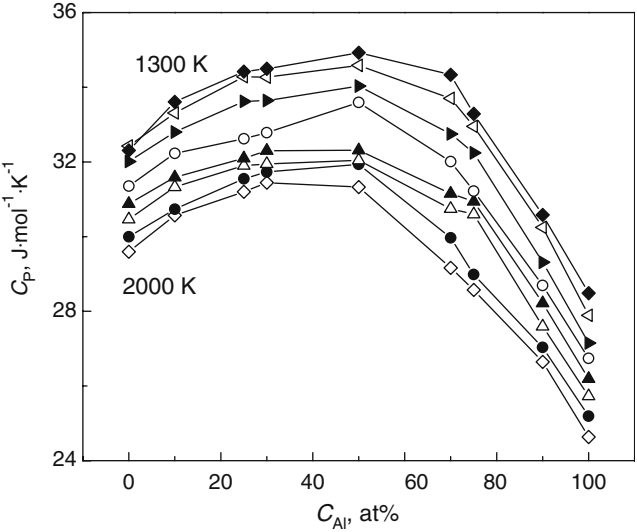

Fig. 5. Dependence of the specific heat on the composition of aluminum.

by Wang et al.[15] within a temperature range including the undercooling regime is also indicated in Fig. 4. The experimentally determined C_P is $30.9 \pm 4.9\,\mathrm{J \cdot mol^{-1} \cdot K^{-1}}$. In fact, this value is an average over the experimentally covered temperature range of 1574 – 2084 K. To facilitate the comparison, we calculate the average specific heat of TiAl alloys within this temperature range by linear regression of the enthalpy. The simulated average specific heat is $32.13 \pm 0.21\,\mathrm{J \cdot mol^{-1} \cdot K^{-1}}$, which is within the error bar of the experimental data, and the difference between these two averaged specific heats is less than 4%. The simulated specific heat of aluminum at the melting point is $32.2\,\mathrm{J \cdot mol^{-1} \cdot K^{-1}}$, which is comparable to the experimentally measured $31.8\,\mathrm{J \cdot mol^{-1} \cdot K^{-1}}$ [16]. The simulated specific heat of titanium at the melting point is $29.7\,\mathrm{J \cdot mol^{-1} \cdot K^{-1}}$, which underestimates the experimentally approximated value of $33.53\,\mathrm{J \cdot mol^{-1} \cdot K^{-1}}$ [17] by about 12%. However, it should be noted that the experimentally measured specific heat of titanium is just an approximation, since the measurement of parameters is too difficult above the melting temperature of titanium. Due to the lack of specific heat data for other Ti–Al alloys for the liquid state, there are no further comparisons.

The composition dependence of the specific heat of Ti–Al alloys is shown in Fig. 5. From the top to bottom, the temperature of the specific heat-composition curve increases from 1300 to 2000 K. With the increase in the aluminum concentration, the specific heat first increases and then

decreases. The peak of the specific heat-composition curve is found at the composition of Ti–50at%Al. Thus, like the case of density, the specific heat of Ti–Al alloys shows a highly nonideal behavior, implying that Neumann–Kopp's rule does not apply to the Ti–Al binary alloy system.

In Figs. 2 and 5, it is also revealed that liquid Ti_3Al, TiAl, and $TiAl_3$ alloys exhibit similar composition dependences of the excess volume and the specific heat as for other non-intermetallic phases. This indicates that although Ti_3Al, TiAl, and $TiAl_3$ are the singular points in the phase diagram, the atomic volume and specific heat do not show obvious irregular behaviors.

5. CONCLUSION

The specific heat and density of Ti–Al alloys from the normal liquid to the undercooled fluid are investigated systematically with molecular dynamics simulations. The simulated data of these two parameters are in reasonable agreement with available experimental data above the melting temperature. Unlike the monotonic change of the density with the addition of aluminum, the specific heat of Ti–Al alloys first increases then decreases with the addition of aluminum, and attains a maximum value at the composition of Ti–50at%Al alloy. The negative value of the calculated excess volume and the composition dependence of the specific heat indicate that liquid Ti–Al alloys deviate from the ideal solution and Neumann–Kopp's rule does not apply to this binary alloy system. Simulations also reveal that those concentrations corresponding to intermetallic phases do not exhibit obvious irregular behaviors in the density and the specific heat.

ACKNOWLEDGMENTS

This work was financially supported by the National Natural Science Foundation of China under Grant Nos. 50395101 and 50371043, and the China Postdoctoral Science Foundation.

REFERENCES

1. C. Cagran, B. Wilthan, G. Pottlacher, B. Roebuck, M. Wickins, and R. A. Harding, *Intermetallics* **11**:1327 (2003).
2. J. Millett, G. T. R. Gray III, and N. Bourne, *J. Appl. Phys.* **88**:3290 (2000).
3. G. Sauthoff, *Intermetallics* **8**:1101 (2000).
4. B. Li, X. Liang, J. C. Earthman, and E. J. Lavernia, *Acta Mater.* **44**:2409 (1996).
5. T. M. Brown and J. B. Adams *J. Non-Crys. Solids* **180**:275 (1995).

6. F. J. Cherne, M. I. Baskes, and P. A. Deymier, *Phys. Rev. B* **65**:024209 (2001).
7. M. Shimono and H. Onodera, *Mater. Sci. Eng. A* **304**:515 (2001).
8. M. Shimono and H. Onodera, *Mater. T. JIM* **39**:147 (1998).
9. Y. Mishin and C. Herzig, *Acta Mater.* **48**:589 (2000).
10. M. S. Daw and M. I. Baskes, *Phys. Rev. Lett.* **50**:1285 (1983).
11. M. S. Daw and M. I. Baskes, *Phys. Rev. B* **29**:6443 (1984).
12. R. R. Zope and Y. Mishin, *Phys. Rev. B* **68**:024102 (2003).
13. J. H. Rose, J. R. Smith, F. Guinea, and J. Ferrante, *Phys. Rev* . B **29**:2963 (1984).
14. T. Iida and R. I. L. Guthrie, *The Physical Properties of Liquid Metals* (Oxford Science Pubs., Oxford, Claredon, 1993), pp. 67–72.
15. N. Wang and B. Wei, *Appl. Phys. Lett.* **80**:3515 (2002).
16. T. Iida and R. I. L. Guthrie, *The Physical Properties of Liquid Metals* (Oxford Science Pubs., Oxford, Claredon, 1993), p. 91.
17. C. J. Smithell, in *Smithells Metals Reference Book,* E. A. Brandes, ed. (Butterworths, London, 1983), pp. 14–13.